A brief review of conductivity and thermal expansion of perovskite-related oxides for SOFC cathode

A.V. Nikonov[*,1], K.A. Kuterbekov[2],
K.Zh. Bekmyrza[2], N.B. Pavzderin[1]

[1]Institute of Electrophysics, Ural Branch, Russian Academy of Sciences, Yekaterinburg, Russia

[2]L.N. Gumilyov Eurasian National University, Astana, Kazakhstan

E-mail: nikonov@iep.uran.ru

Cathode materials with mixed ion-electron conductivity (MIEC) are necessary for the development of low or intermediate temperature solid oxide fuel cells. Perovskite and perovskite-related materials are promising candidates on this role. In the review the conductivity and the thermal expansion of materials with various types of perovskite-related structures such as pure perovskite, double perovskite, brownmillerite and Ruddlesden-Popper phases have been compared. And the literature data on the values of the electronic and ionic conductivities, the oxygen diffusion coefficient, and the thermal expansion coefficient of various compositions have been collected. It was shown that the disordered cubic perovskites possess the higher electronic conductivity whereas the layered perovskites and materials with the Ruddlesden-Popper structure have higher ionic conductivity and lower value of thermal expansion.

Keywords: cathode, perovskite-related structure, electronic and ionic conductivity, thermal expension, SOFC.

Introduction

Solid oxide fuel cells (SOFCs) are high-temperature devices for direct electrochemically converting chemical energy of fuel into electrical energy and heat.

SOFC possess several advantages: high electrical efficiency, fuel versatility, noise-free nature, and low-pollutant emission [1].

The operation principle of an SOFC is shown in Figure 1. A fuel cell consists of two porous electrodes (the anode and cathode) separated by a gastight electrolyte. Fuel is fed to the anode where it is oxidized and electrons are released to the external circuit. Oxidant is fed to the cathode where it is reduced and electrons are accepted from the external circuit. The electron flow (from the anode to the cathode) through the external circuit produces direct-current electricity. The electrolyte conducts oxygen ions between the two electrodes.
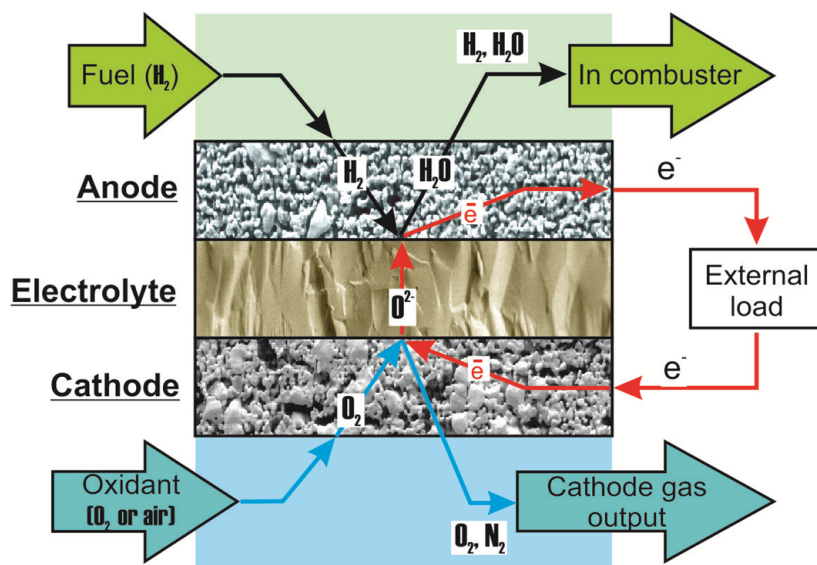

Figure 1. The operation principle of the SOFC.

High operating temperatures of SOFC allow, first, to avoid the use of expensive catalysts based on noble metals; second, to use practically any hydrocarbons as a fuel; thirdly, to have low internal resistance, and, consequently, high power. The internal resistance of SOFC consists of three types of resistances: ohmic, polarization (or activation) and concentration (or diffusion) ones. The specific electrical resistance of materials of the SOFC components and their geometry (thickness, porosity) are responsible for the ohmic resistance, the one's magnitude of which increases with current growth, in accordance with Ohm's law. Polarization resistance is associated with the complexity of oxidation-reduction reactions on electrodes that occur with a change in the charge carrier. Concentration resistance arises by difficulties in supplying initial gaseous reagents and/or removing reaction products from electrodes and makes a significant contribution to total losses only at high current, when the rates of electrochemical processes become significant. The ohmic and polarization resistances have thermal activation nature therefore their values drop with temperature increasing.

On the other hand the same high operating temperature results in several technological hurdles (slowly start-up, strict requirements for SOFC materials, degradation processes) and hinders commercialization of this technology [2]. Therefore, in recent years, great efforts have been devoted to develop low or intermediate temperature SOFCs (LT-SOFC or IT-SOFC) operating below 800

°C while maintaining a high specific power. However, a decrease of the operating temperature inevitably leads to an increase in the ohmic and polarization resistances, which negatively affect the power of the device. Especially it affects the oxygen reduction reaction (ORR) at the cathode during which strong double bond in the oxygen molecule is broken to form O^{2-} ion. For example, in the works [3, 4] it is shown that losses caused by cathode processes can be up to 65% from total voltage drop of the fuel cell. Thus, the development and optimization of stable and high activity cathodes become one of the main performance-limiting factors of IT-SOFCs.

The traditional, well-studied cathode material of SOFC is lanthanum strontium manganite $La_{1-x}Sr_xMnO_{3-\delta}$ (LSM) [5]. This material is characterized by high stability, compatibility with electrolyte $Zr_{1-x}Y_xO_{2-\delta}$ (YSZ) [6] and enough high electronic conductivity (for $La_{0.8}Sr_{0.2}MnO_{3-\delta}$ at 900 °C σ_e =300 Sm × cm^{-1} [7]). In comparison with electron conductivity, the ionic conductivity of the LSM is negligible (for $La_{0.8}Sr_{0.2}MnO_{3-\delta}$ at 1000 °C $\sigma_i \sim 5.76 \times 10^{-6}$ Sm × cm^{-1} [8]). Therefore, the oxygen reduction reaction may occur only near the triple phase boundary (TPB) which is the contact sites of three phases: electrolyte (ionic conductor), electrode (electronic conductor) and gas. The rate of the cathode reaction, which determines the value of the polarization resistance (R_η), depends on TPB length.

There are two ways of extension of TPB: 1) formation of a composite electrode and optimization of its structure (including creation of nanostructure by impregnation) [9-11] and 2) use of a mixed ion-electron conductor (MIEC) as cathode material [10, 12, 13]. The possibility of the electrode characteristic enhancement of a composite cathode has certain limit connected with the optimum ratio of electrode and electrolyte. Therefore, the most promising method to create the desired cathode is search of novel MIEC materials.

In view of the foregoing, for an efficient operation of SOFC, the cathode should possess the following characteristics [14]:

- High electronic conductivity (preferably more than 100 S/cm in an oxidizing atmosphere [15]);

- Minimum or no mismatch between the values of the thermal expansion coefficient (TEC) of the cathode and other components of the cell, such as, electrolyte, and interconnect materials;

- Good chemical compatibility with the electrolyte and interconnect materials;

- Sufficient porosity to allow fast diffusion of O_2 gas from cathode to cathode-electrolyte interface;

- High oxide ion conductivity;

- Good stability under an oxidizing atmosphere in the course of fabrication as well as operation;

- High catalytic activity during oxygen reduction reaction (the desired value of the polarization resistance R_η is less than 0.15 $\Omega \times cm^2$ [16]);

- Cost effective.

The suitability of mixed conducting materials to use as the SOFC cathode can be estimated by the Adler-Lane-Steele model [17]. Within the framework of the model, the polarization resistance of the cathode determined as resistance of heterogeneous chemical reaction at the gas-electrode interface is related to its characteristics:

$$R_\eta = \frac{RT}{2F^2} \sqrt{\frac{\tau}{(1-\epsilon)\alpha C_0^2 D^* k}}, \tag{1}$$

where $R = 8.314 \, \text{J} \times \text{mol}^{-1} \times \text{K}^{-1}$, F = 96485.33 $\text{C} \times \text{mol}^{-1}$, T is temperature, τ, ϵ, α are tortuosity, fractional porosity, and internal surface area/unit volume, respectively, C_0 is the surface concentration of oxygen, D^* is the oxygen self-diffusion coefficient and k is oxygen surface exchange coefficient. The values of D^* and k, which are acceptable for the cathode material, have been evaluated in [18]. Assuming that $R_\eta = 0.1 \, \Omega \times \text{cm}^2$ and substituting in (1) typical parameters of the cathode microstructure, it was found that the product $D^* k$ should be of the order of 10^{-14}. Thus, taking into account that the oxygen surface exchange coefficient at SOFC operating temperatures does not exceed 10^{-6} $\text{cm} \times \text{s}^{-1}$, the value of D^* for a cathode material should be not less than $10^{-8} \, \text{cm} \times \text{s}^{-1}$.

The data on D^{**} and k various complex oxides were collected in [14, 19] and it was shown that many materials with the perovskite structure or its derivatives satisfy the above requirement. Consequently perovskite-type materials are promising applicants for the role of a cathode for intermediate temperature SOFCs.

The present work focuses on relation of the electron and ionic conductivity and thermal expansion of perovskite and perovskite-related materials with their structure.

Perovskite and perovskite-related structure

Materials with perovskite structure (ABO_3) are one of the most widespread families of complex oxides. A- and B-site cations having different crystallochemical characteristics allow changing the chemical composition of the phase within a wide range. Compositional variations cause significant modifications of both their crystal and electronic structure, having a great impact in their physical properties. In addition the accommodation of multiple cations onto the A and/or B sites of the structure and ordering effects of the ions and non-stoichiometry can significantly affect on the properties of the perovskite-type materials.

In the literature, several thorough reviews on the description of the perovskite and perovskite-related structures are presented [20-25]. Therefore, in the section we present only brief description of these structures.

Perovskite structure

The idealised or aristotype cubic ABO3 perovskite structure (space group $Pm\bar{3}m$) is shown in Figure 2 [21]. The B cations are located at the corners and the A cations at the center of the unit cell. The oxygen is placed at the centers of the twelve cube edges giving corner-shared strings of BO6 octahedra which extend infinitely in three dimensions. The coordination numbers of A- and B-site cations are 12 and 6, respectively. The ion radius of A-site cations is close to anion one therefore large low-charge ions of alkaline, alkaline-earth and rare-earth metals can perform as A cation. The B-site cations usually represent medium-sized ions of transition metals.

Although few compounds have this ideal cubic structure, many oxides have slightly distorted variants with lower symmetry (e.g., hexagonal or orthorhombic). The deviation from the ideal structure in perovskite oxides can be expressed through the tolerance factor (t) which was first used by Goldschmidt in 1926 [26]:

$$t = \frac{r_A + r_O}{\sqrt{2}(r_B + R_O)},\tag{2}$$

where r_A, r_B and r_O are ion radii of A-, B-site cations and anion, respectively.

Ideally t should be equal to 1.0 and it has been found empirically that if t lies in the approximate range 0.9-1.0 a cubic perovskite structure is a reasonable possibility. If $t > 1$, i.e. large A and small B, a hexagonal packing of the AO_3 layers is preferred and hexagonal phases of the $BaNiO_3$ type form. In cases where t of the order of 0.71-0.9, the structure, particularly the octahedral framework, distorts to close down the cuboctahedral coordination polyhedron, which results in a crystal structure of lower symmetry than cubic [27-29]. For even lower values of t, the A and B cations are of similar size and are associated with the ilmenite structure [30].

The degree of the perovskite structure distortion which affected on the material properties can be modify by partial substitution of A- and/or B-site cations ($A_{1-x}A'_x BO_3$, $AB_{1-x}B'_x O_3$ and $A_{1-x}A'_x B_{1-y}B'_y O_3$). For example, most of the undoped perovskite materials are poor oxide ion conductor in air. On partially substituting the A-site cation (or B-site cation) with acceptor cations results in the formation of oxygen vacancies and hence in an increase in ionic conductivity. However in some cases when charges or the ionic radii of host- and dopant-cations differ enough, lattice energy can often be reduced by ordering some or all of the ions over the available crystallographic sites. Thus, ordered perovskites are formed.

Ordered perovskite structure

Partial cation substitution is a very common method for tailoring the properties of perovskite compounds. This substitution can take place either at the A or the B site, and in varying degrees. However, in the case where exactly half of the A- or B-site cations are substituted with another cation the structure ordering can occur. Thus, the so-called double perovskites are formed. Their general formula
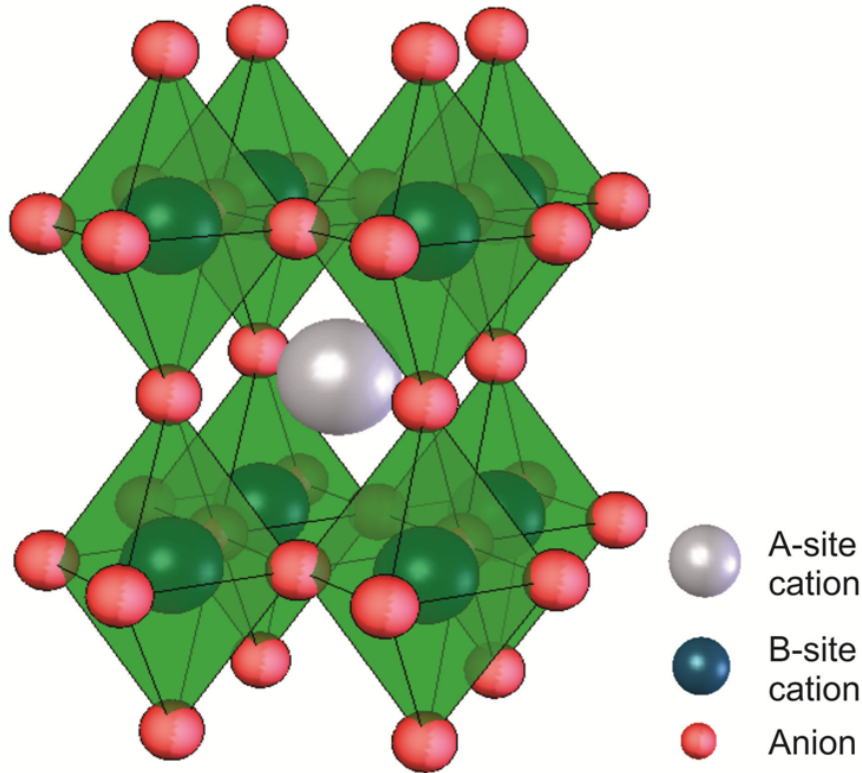
Figure 2. The cubic ABO_3 perovskite structure.

can be written as $A_{0.5}A'_{0.5}BO_{3-\delta}$ (or $AB_{0.5}B'_{0.5}O_{3-\delta}$). However when the size difference between the two cations is significant they tend to order and the formula for the material is rewritten in the following manner $AA'B_2O_{5+\delta}$ (or $A_2BB'O_{5+\delta}$). The detailed description of $A_2BB'O_6$ perovskites is represented elsewhere [22].

There are three simple patterns of ordering that can be envisioned for either the A- or B-site cations [21]. The most symmetric is called rock salt ordering because the pattern of B and B' (or A and A') cations is equivalent to the anion and cation positions in the rock salt structure. In addition to the rock salt ordering, cations can order into columns, or layers as shown in Figure 3. As a general rule B-site cations order more readily than A-site cations. When cation ordering does occur, rock salt ordering of B/B' cations is favored in $A_2BB'O_6$ perovskites, whereas layered ordering of A/A' cations is favored in $AA'B_2O_6$ and $AA'BB'O_6$ perovskites. The reasons and conditions of all types of perovskite ordering are described in detail in [21].

Along with the cations ordering in the perovskite structure at a high oxygen deficit the anions ordering can also be observed. Thus brownmillerite structure (general formula $A_2B_2O_5$ or $ABO_{2.5}$) can be thought of as an ABO_3 perovskite with one-sixth of the oxygen atoms removed [24, 25]. As can be seen from Figure 4 the brownmillerite structure consists of alternating perovskite layers of corner-sharing BO_6 octahedra and BO_4 tetrahedra. The ordered anion vacancies form the parallel rows of along the [110] crystallographic direction. The aristotype brownmillerite structure (space group Imma) is high symmetric. However the Imma structure can be disordered due to rotations of the octahedra and twist of

the tetrahedral chains [25].
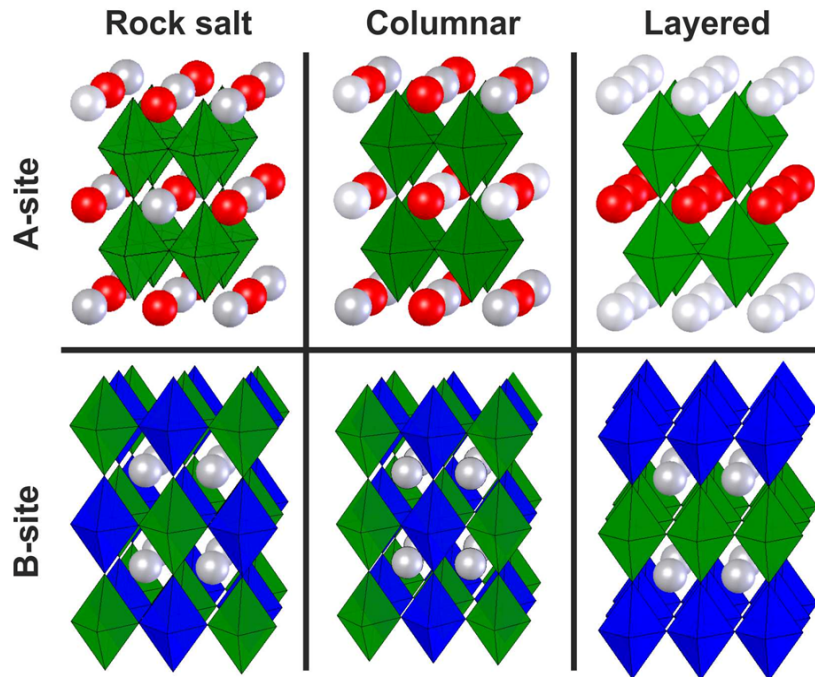
Figure 3. Cation ordering schemes in perovskites. From left to right rock salt, columnar ordering and layered ordering are shown for A-site ordering in AA'B2O6 (top) and B-site ordering in A2BB'O6 perovskites (bottom).

Figure 4. Crystal structure of brownmillerite $A_2B_2O_5$ (or $ABO_{2.5}$) where layers of BO_6 octahedra alternate with BO_4 tetrahedra.

Ruddlesden-Popper phases structure

Another interesting from the point of view of the cathode material the phases related to the perovskite structure are Ruddlesden-Popper phases (RP) which

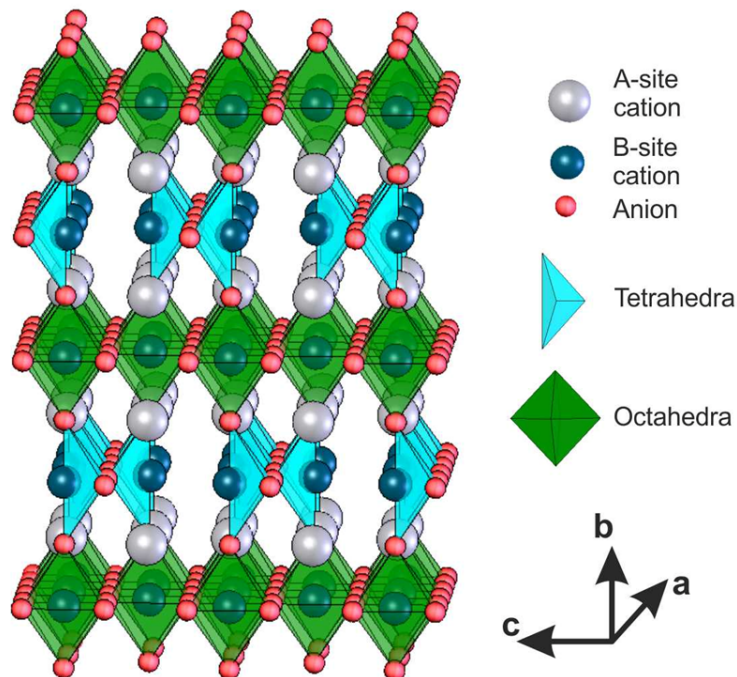are described with the general formula of $A_{n+1}B_nO_{3n+1}$ (n = 1, 2, 3). [31]. These phases have modular in nature, being built from n ABO_3 perovskite layers are sandwiched between two AO rock-salt layers and are arranged along the c-axis (Figure 5) [32]. The simplest member of the series, A_2BO_4 (n= 1), adopts the K_2NiF_4 structure. Increasing the perovskite layers thickness while keeping the inter-layers structure the same generates the phases $A_3B_2O_7$ (n = 2) and $A_4B_3O_{10}$ (n = 3).
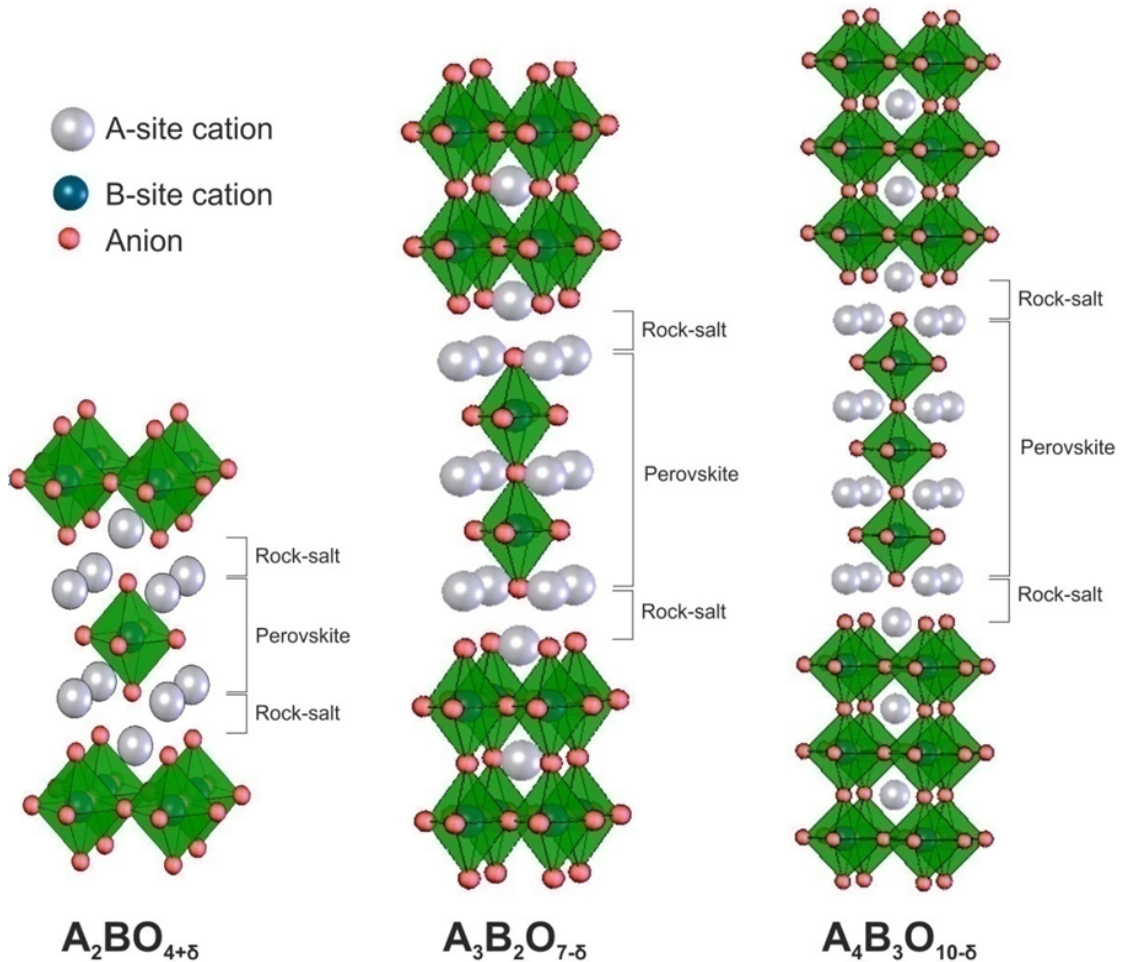
Figure 5. The structure of Ruddlesden-Popper phases ($A_{n+1}B_nO_{3n+1}$ where n = 1, 2, and 3).

In practice, many phases are disordered and contain random or partly ordered wider or narrower bands of perovskite-like structure corresponding to different n values. Non-stoichiometry is common for phases containing Co, Mn or Fe as the B-site cation. In addition, octahedral tilting and distortion are present in the perovskite layers, and these both lower the symmetry of the structures and influence their physical properties [30].

Electronic conductivity

The electron conduction nature is similar for all perovskite-related structures. It is assumed that the B-O-B bond is responsible for electrical properties [33]. The BO_6 octahedra build up a network throughout the perovskite structure and

electronic conduction proceeds via electrons or holes along the B-O-B chains. The interaction between the B-site cation d-orbitals and the oxygen ion 2p-orbitals causes the electron/hole exchange. Thus perovskite-related oxides containing transition metals with incompletely filled d-orbital as B-site cation can have high electrical conductivity. In the case of the cubic structure perovskite the orbitals overlap is most effective whereas the overlap degree decreases with distortion of the perovskite structure that result in reducing of the conductivity. Therefore, taking into account the aforesaid tolerance factor, among the ABO_3 perovskites, the highest electronic conductivity should be inherent in compositions with a large A-site cation such as La and Pr [19].

Moreover, in accordance to the above double exchange mechanism, to achieve high electronic conductivity it requires B-site cation with multiple valences [19, 34]. The electronic conduction can be of n-type or p- type, depending on the material properties and the ambient oxygen partial pressure. The n-type electronic conductors are generally not stable at high temperatures in air or other oxidizing atmospheres since an oxygen deficiency is required to generate electrons. However, p- type electronic conductors are typically stable in air because an excess of oxygen is required to generate holes [35]. Thus the most favorite suitable candidates for the B-site cation are Cr, Mn, Fe, Co, Ni. The cobalt-, manganese- and nickel-containing oxides possess the higher electrical conductivity (Table 1).

In addition the electronic conductivity of the perovskite can be changed influenced by partly substituting ions on the A-site and/or on the B-site. At isovalent substitution the dopant ions (A′ and/or B′) affect the electronic conductivity due to ionic radii. The small ions result in distortion of the perovskite structure and respectively in decrease of the electronic conductivity. At aliovalent substitution on the A-site cations when the ions differ in both valences and so on the radii a more complex situation arises. To maintain electrical neutrality, the valence change introduced by the A-site has to be compensated either by a multivalent B-site cation (transition metal) or by creating vacancies on the oxygen sublattice. The radius of the transition metal also depends on its valence state. However, it is known that substitution for La^{3+} with ions of alkaline-earth elements of Ca^{2+}, Sr^{2+}, Ba^{2+} improves the electronic conductivity [35]. It should be borne in mind that the reactivity of alkaline-earth metal oxides increases with the transition from calcium to barium. Thus, the disadvantage of the barium-containing perovskites is the chemical interaction with the electrolytes and CO_2 contained in the air.

From a comparison of the electronic conductivity data presented in Tables 1-3, it is seen that the La-Co compositions with a disordered cubic structure possess highest electronic conductivity whereas the conductivity of the ordered perovskites and the Rudlessden-Popprea phases is much lower. In finishing of this section it would like to note the detailed review [36] summarizing conductivity data of huge amount of compositions with layered perovskite structure.

Table 1.
Composition, electrical conductivity σ_e, ionic conductivity σ_i, oxygen diffusion coefficient D^*, oxygen surface exchange coefficient k, and TEC of disordered perovskites.

Material	T_σ, °C	σ_e, S·cm⁻¹	σ_i, S·cm⁻¹	T_{D+k}, °C	D^*, cm²·s⁻¹	k, cm·s⁻¹	T_{TEC}, °C	TEC (×10⁻⁶), K⁻¹	Reference
$LaMnO_3$	950	115		800	7.7×10^{-15}	9.2×10^{-9}	25-1100	11.2	[37, 38]
$LaFeO_3$				900	9.84×10^{-13}	3.89×10^{-8}			[39, 40]
$LaCoO_3$	700	1024.4		800	2.41×10^{-11}	3.47×10^{-7}	100-700	23.5	[41, 42]
$LaCrO_3$	1000	1						9.5	[40]
$LaCo_{0.8}Fe_{0.2}O_3$	800	150	4×10^{-3}						[43]
$La_{0.8}Sr_{0.2}MnO_3$	900	300	5.93×10^{-7}	800	4.0×10^{-15}	5.6×10^{-9}		11.8	[13]
$La_{0.8}Sr_{0.2}FeO_3$	800	100.5					100-900	12.6	[44]
$La_{0.8}Sr_{0.2}CoO_3$	800	1521		800	2.0×10^{-8}	5.0×10^{-6}	30-1000	18.5	[19, 45]
	800	1238					100-900	19.7	[44]
$La_{0.7}Sr_{0.3}CoO_3$	800	1676					30-1000	19.2	[45]
$La_{0.7}Sr_{0.3}CrO_3$	700	15						19	[40]
$La_{0.65}Sr_{0.35}MnO_{3-\delta}$	800	102.3	1.7×10^{-4}	900	4.0×10^{-14}	5.0×10^{-8}	30-1000	12.3	[19, 46]
$La_{0.6}Sr_{0.4}MnO_3$	730	200					30-830	11.7	[52]
$La_{0.6}Sr_{0.4}FeO_3$	800	129	5.6×10^{-3}				30-1000	16.3	[46]
$La_{0.6}Sr_{0.4}CoO_3$	800	1585	0.22					20.5	[46]
$La_{0.5}Sr_{0.5}MnO_3$	950	300							[37]
$La_{0.5}Sr_{0.5}CoO_3$	800	1356					30-1000	22.3	[45]
	800	1349	0.093				30-1000	22.3	[46]
$La_{0.8}Sr_{0.2}Mn_{0.5}Co_{0.5}O_3$	800	190					20-1000	15	[47, 48]
$La_{0.8}Sr_{0.2}Fe_{0.9}Co_{0.1}O_{3-\delta}$	800	31.6	2.2×10^{-3}				30-1000	13.9	[46]
$La_{0.8}Sr_{0.2}Fe_{0.8}Co_{0.2}O_{3-\delta}$	800	87	2.3×10^{-3}				30-1000	14.8	[46]
		153.9					100-900	15.4	[44]
$La_{0.8}Sr_{0.2}Fe_{0.7}Co_{0.3}O_{3-\delta}$	800	228.5					100-900	16.5	[44]
$La_{0.8}Sr_{0.2}Fe_{0.6}Co_{0.4}O_{3-\delta}$	800	292.5					100-900	17.6	[44]
$La_{0.8}Sr_{0.2}Fe_{0.5}Co_{0.5}O_{3-\delta}$	800	331.6					100-900	18.7	[44]
	800	354.8					30-1000	17.6	[46]
$La_{0.8}Sr_{0.2}Co_{0.6}Fe_{0.4}O_{3-\delta}$	800	456					100-900	20.0	[44]
$La_{0.8}Sr_{0.2}Co_{0.7}Fe_{0.3}O_{3-\delta}$	800	776					100-900	20.3	[44]
$La_{0.8}Sr_{0.2}Co_{0.8}Fe_{0.2}O_{3-\delta}$	800	1000	0.04				30-1000	19.3	[46],
	800	1003.5					100-1000	20.7	[44]
$La_{0.8}Sr_{0.2}Co_{0.9}Fe_{0.1}O_{3-\delta}$	800	1071					100-900	20.1	[44]
$La_{0.75}Sr_{0.2}Mn_{0.8}Co_{0.2}O_{3-\delta}$	800	79.4	1.7×10^{-4}				30-1000	9.5	[46]
$La_{0.7}Sr_{0.3}Fe_{0.8}Co_{0.2}O_3$	800	159					30-1000	16.0	[45]
$La_{0.7}Sr_{0.3}Cr_{0.5}Co_{0.5}O_3$	700	58						19	[40]
$La_{0.65}Sr_{0.3}Fe_{0.8}Co_{0.2}O_{3-\delta}$	800	158.8	4×10^{-3}				30-1000	14.9	[46]
$La_{0.6}Sr_{0.4}Mn_{0.8}Fe_{0.2}O_3$	730	39					30-830	11.3	[52]
$La_{0.6}Sr_{0.4}Mn_{0.8}Ni_{0.2}O_3$	730	160					30-830	12.7	[52]
$La_{0.6}Sr_{0.4}Fe_{0.8}Co_{0.2}O_3$	800	302	8×10^{-3}	850	7.4×10^{-8}	2.4×10^{-5}	30-1000	17.5	[46, 49]
$La_{0.6}Sr_{0.4}Fe_{0.5}Co_{0.5}O_3$	800	489.8					30-1000	20.3	[46]
$La_{0.6}Sr_{0.4}Co_{0.8}Fe_{0.2}O_3$	800	269	0.058				30-1000	21.4	[46]
$La_{0.6}Sr_{0.4}Ni_{0.6}Co_{0.4}O_{3-\delta}$	800	77.6		800	7.0×10^{-8}	2.0×10^{-6}			[50]
$La_{0.8}Ca_{0.2}CrO_3$	700	7.1							[40]
$La_{0.5}Ca_{0.5}MnO_3$	800	~260					100-900	11.4	[51]
$PrCrO_3$	1000	0.18					30-900	8.5	[52]
$Pr_{0.8}Sr_{0.2}Fe_{0.8}Co_{0.2}O_{3-\delta}$	800	76	1.5×10^{-3}				30-1000	12.8	[46]
$Pr_{0.8}Sr_{0.2}Mn_{0.8}Co_{0.2}O_{3-\delta}$	800	83.2	3×10^{-5}				30-1000	10.9	[46]
$Pr_{0.75}Sr_{0.25}Mn_{0.8}Co_{0.2}O_{3-\delta}$	800	95.5	1.1×10^{-4}				30-1000	10.8	[46]
$Pr_{0.7}Sr_{0.3}Mn_{0.8}Co_{0.2}O_{3-\delta}$	800	199.5	4.4×10^{-5}				30-1000	11.1	[46]
$Pr_{0.68}Sr_{0.3}Fe_{0.8}Co_{0.2}O_3$	800	171					25-600	12.4	[53]
$Pr_{0.65}Sr_{0.3}MnO_{3-\delta}$	800	209	3.4×10^{-4}				30-1000	11.6	[46]
$Sr_{0.9}Ce_{0.1}FeO_{3-\delta}$	800	28.8	0.064				30-1000	20.2	[46]
$Sr_{0.9}Ce_{0.1}CoO_{3-\delta}$	800	295	0.133				30-1000	21.5	[46]
$Sr_{0.9}La_{0.1}CoO_3$	800	191					30-1000	26	[45]
$Sr_{0.7}La_{0.3}CoO_{3-\delta}$	800	912	0.76				30-1000	25.0	[46]
$Sr_{0.7}La_{0.3}FeO_3$	800	44					30-1000	25.6	[45]
$Sr_{0.6}La_{0.4}CoO_3$	800	1156					30-1000	25.1	[45]
$Sr_{0.9}Ce_{0.1}Fe_{0.8}Ni_{0.2}O_{3-\delta}$	800	87.1	0.04				30-1000	18.9	[46]
$Sr_{0.85}Ce_{0.15}Fe_{0.8}Co_{0.2}O_{3-\delta}$	800	38.9	0.016				30-1000	18.5	[46]
$Sr_{0.7}La_{0.3}Co_{0.9}Fe_{0.1}O_3$	800	837					30-1000	19.2	[45]
$Sr_{0.7}La_{0.3}Co_{0.7}Fe_{0.3}O_3$	800	217					30-1000	24.7	[45]
$Sr_{0.7}La_{0.3}Co_{0.5}Fe_{0.5}O_3$	800	124					30-1000	23.5	[45]
$Sr_{0.7}La_{0.3}Fe_{0.7}Co_{0.3}O_3$	800	54					30-1000	27.1	[45]
$Sr_{0.7}La_{0.3}Fe_{0.9}Co_{0.1}O_3$	800	61					30-1000	24.8	[45]
$SmCrO_3$	1000	0.39					30-900	8.6	[52]
$Sm_{0.68}Sr_{0.3}Fe_{0.8}Co_{0.2}O_3$	800	43.4					25-600	13.7	[53]
$NdCrO_3$	1000	0.17					30-900	8.3	[52]
$Nd_{0.68}Sr_{0.3}Fe_{0.8}Co_{0.2}O_3$	800	106.9					25-600	13.4	[53]
$Ba_{0.68}Sr_{0.3}Fe_{0.8}Co_{0.2}O_3$	800	9.3					25-600	20.2	[53]

Table 2.

Composition, electrical conductivity σ_e, ionic conductivity σ_i, oxygen diffusion coefficient D^*, oxygen surface exchange coefficient k, and TEC of disordered perovskites.

Material	T_σ, °C	σ_e, S·cm⁻¹	σ_i, S·cm⁻¹	T_{D^*k}, °C	D^*, cm²·s⁻¹	k, cm·s⁻¹	T_{TEC}, °C	TEC (×10⁻⁶), K⁻¹	Reference
$LaBaCo_2O_{5+\delta}$	700	1076					80-900	24.3	[54]
$LaSrCoMnO_{5+\delta}$	700	124						15.8	[55]
$PrBaCo_2O_{5+\delta}$	700	695		500	3.6×10^{-7}	6.9×10^{-5}		20.4	[56, 57]
	700	932		580	4.2×10^{-6}	3.4×10^{-4}			[58]
				300	1.7×10^{-11}	3.49×10^{-9}			[59]
$PrBaCoFeO_{5+\delta}$	700	163					80-900	21.0	[60]
$PrBaFe_2O_{5+\delta}$	700	7.1						17.2	[61]
$SmBaCo_2O_{5+\delta}$	700	633					80-900	17.1	[54]
$SmSrCo_2O_{5+\delta}$	700	502						22.7	[62]
$GdBaCo_2O_{5+\delta}$	700	388					80-900	16.6	[54]
	750	925		500	2.8×10^{-7}	7.5×10^{-5}			[57]
	500		0.01	520	2.75×10^{-8}	9.3×10^{-8}			[63]
				496	2.8×10^{-10}	7.4×10^{-8}			[64]
	825		5×10^{-5}	825	9×10^{-11}				[65]
				350	3×10^{-7}	2×10^{-4}			[66]
$NdBaCo_2O_{5+\delta}$	700	388		600	1.23×10^{-14}		80-900	16.6	[54, 59]
$YBaCo_2O_{5+\delta}$	700	120					80-900	15.8	[54]
$SmSrCo_{1.4}Mn_{0.6}O_{5+\delta}$	700	110					80-900	18.1	[62]
$SmSrCoMnO_{5+\delta}$	700	45.9					80-900	13.8	[62]
Browmellerit									
$Ba_2In_2O_5$	700		5×10^{-3}						[67]
$Ca_2Cr_2O_5$	700		5×10^{-3}						[67]
$Ca_2Fe_2O_5$	600	~0.3					100-680	13.1	[68]
Sr_2ScAlO_5	700		1×10^{-5}						[67]
Ca_2FeAlO_5	850	~0.03	6.65×10^{-5}						[68]

Table 3.

Composition, electrical conductivity σ_e, ionic conductivity σ_i, oxygen diffusion coefficient D^*, oxygen surface exchange coefficient k, and TEC of Ruddlesden-Popper phases. * porous samplen; ** - vacancy diffusion coefficient.

Material	T_σ, °C	σ_e, S·cm⁻¹	σ_i, S·cm⁻¹	T_{D^*k}, °C	D^*, cm²·s⁻¹	k, cm·s⁻¹	T_{TEC}, °C	TEC (×10⁻⁶), K⁻¹	Reference
La_2NiO_4	800	~47		800	1.2×10^{-7}	1.7×10^{-6}	20-1000	13.0	[69]
				800	1.71×10^{-7}	2.55×10^{-6}			[19]
				700	3.38×10^{-8}	1.75×10^{-7}	300-1000	13	[70]
	750	65		500	3.3×10^{-9}	7.0×10^{-9}			[57]
$La_2CoO_{4+\delta}$	750	5		500	2.5×10^{-8}	3.2×10^{-6}			[57]
La_2CuO_4	800	6.3		700	~1×10^{-8}	~1×10^{-6}		10.6	[19, 71]
				700	5×10^{-9}	1.6×10^{-6}			[70]
$Pr_2NiO_{4+\delta}$	800	~94		800	1.2×10^{-7}	3.1×10^{-6}	20-1000	13.6	[69]
				700	7.94×10^{-8}	1.73×10^{-6}	300-1000	13.6	[70]
Pr_2CuO_4				700	7.2×10^{-13}	1.2×10^{-8}	300-1000	10.2	[19, 70]
$Nd_2NiO_{4+\delta}$	800	~34		800	1.0×10^{-7}	7.6×10^{-7}	20-1000	12.7	[69]
				700	5.0×10^{-8}	3.98×10^{-7}			[70]
$Nd_2CuO_{4+\delta}$				700	3.3×10^{-9}				[70]
$La_{1.9}Sr_{0.1}NiO_4$				800	2.1×10^{-8}	8.7×10^{-6}			[69]
$La_{1.9}Sr_{0.1}NiO_4$				800	2.2×10^{-8}	2.2×10^{-7}			[69]
				800	1.33×10^{-8}	6.46×10^{-7}			[72]
$La_{1.7}Sr_{0.3}NiO_4$	800	80						11.3	[73]
$La_2Ni_{0.8}Co_{0.2}O_{4+\delta}$				800	9.8×10^{-8}	2.2×10^{-6}		11.3	[69]
$La_2Ni_{0.7}Co_{0.3}O_{4+\delta}$				700	5.46×10^{-8}	6.26×10^{-5}			[74]
$La_2Ni_{0.9}Fe_{0.1}O_{4+\delta}$				800	1.0×10^{-7}	1.7×10^{-6}		11.3	[69]
$LaSrCoO_{4-\delta}$	800	141						14.3	[70]
$La_{0.9}Sr_{1.1}FeO_{4-\delta}$	800							10.2	[70]
$Nd_{1.8}Ca_{0.2}NiO_{4+\delta}$	800	~71		800	1.8×10^{-8}	7.6×10^{-7}			[69]
High-order Ruddlesden–Popper phases									
$La_3Ni_2O_{7-\delta}$*	800	52*						13.7	[75]
$La_4Ni_3O_{10-\delta}$*	800	86*						13.5	[71, 75]
$Sr_3Fe_2O_{7-\delta}$	900	26	0.015	900	1.8×10^{-7}**				[76]
	900	20.7	0.018						[77]
	900		0.018						[78]
$Sr_3Fe_{1.9}Sc_{0.1}O_{7-\delta}$	900	12.3	0.023						[78]
$Sr_3Fe_{1.7}Sc_{0.3}O_{7-\delta}$	900	5.9	9.8×10^{-3}						[78]
$Sr_{2.7}La_{0.3}Fe_2O_{7-\delta}$	900	31	0.005	900	2.3×10^{-7}**				[76]
$Sr_{2.7}La_{0.3}Fe_{1.4}Co_{0.6}O_{7-\delta}$	900	50	0.025	900	8.9×10^{-7}**				[76]
$Sr_{2.7}La_{0.3}FeCoO_{7-\delta}$	900	78	0.045	900	1.3×10^{-6}**				[76]

Ionic conductivity

The ionic conductivity of MIEC perovskites is usually several orders of magnitude less than that of the electronic component. The vacancy mechanism being assumed is the basis for the oxygen-ion conductivity of perovskites. The value of the ionic conductivity can be determined from the concentration (n) and the mobility (μ) of the oxygen vacancies according to the expression:

$$\sigma_i = ne\mu, \tag{3}$$

where e is unit charge. However measurement of the ionic conductivity is enough difficult and the literature data on its exact values are few. Therefore along with σ_i the data on the oxygen self-diffusion coefficient (D^*) are collected in Table 1. According to the Nernst-Einstein equation, the self-diffusion coefficient is proportional to the ionic conductivity. However in work [79] it states that the introduction of dopants does not affect on the oxygen vacancies mobility.

Thus, to achieve high oxygen-ion conductivity, it is required to increase the mobility and concentration of the oxygen vacancies. The substitution of the A-site and/or B-site cations with ions having lower valence allows increasing the oxygen vacancies concentration. In such event the nature of B-site cation is important parameter. As mentioned above, at the aliovalent substitution of A-site cations the electroneutrality of the structure can be preserved without the oxygen vacancies formation if B-site cation is multivalent. An example is comparison of the transport characteristics changes of La-Co and La-Mn systems at substitution of La^{3+} by Sr^{2+}. As can be seen from Table 1, the ionic conductivity of $La_{1-x}Sr_xMnO_3$ increases insignificantly with increasing of x, because the electroneutrality is preserved by the electronic compensating mechanism [80].Whereas the oxygen diffusion coefficient of $La_{1-x}Sr_xCoO_3$ grows by 3 orders of magnitude already at $x = 0.2$ due to the oxygen deficiency of these compositions [81].

Along with the chemical composition the structure of the crystal lattice is another important parameter that affects the ionic conductivity of perovskites. By the example of electrolyte compositions $La_{1-x}Sr_xGa_{1-y}Mg_yO_{3-\delta}$ it was showed that the highest conductivity is registered at the tolerance factor close to 0.96 [82]. It assumes that at this value of t the stress-free lattice with the oxygen vacancies having highest mobility and lowest activation energy is realized [83]. Whereas a strong lowering of the lattice symmetry will result in drop of the oxygen mobility due to the noncrystallographic equivalence of the different vacancy and oxygen sites. The proof of this is found in [84] where it was shown that the conductivity decreases linearly with the deviation of the tolerance factor from the ideal value.

In the cubic closest packing of the ideal perovskite, the A-site cations should be equal in size to the anion, implying that the A-site cation radius (r_A) is 1.40 Å. This explains why La^{3+} ($r_{La} = 1.36$ Å at CN=12) and Sr^{2+} ($r_{Sr} = 1.44$ Å) usually are the best A-site ions for maximizing the conductivity. In a defect-free perovskite lattice the radius of B-site cation should be the "radius" of the octahedral hole $r_{oh} = 0.58$ Å [83]. Taking into account the fact that the B-O

octahedra constitute the framework of the perovskite structure, and the oxide bonding to the small B-ion is much stronger than to the large A-ion the optimum oxide ion conductor should be found among the $A^{3+}B^{3+}O_3$-type of perovskites [82, 84]. The interaction between the B-site ion and the anion is expected to increase in $A^{2+}B^{4+}O_3$ and even more in $A^{1+}B^{5+}O_3$. In addition, a number of $A^{2+}B^{4+}O_3$ oxides (for example, $SrCeO_3$ and $BaCeO_3$ [85, 86]) are proton and not oxygen ionic conductors. Thus, as in the case of electron conduction, the most favorite suitable candidates for the B cation are the following ions: Co^{3+} ($r_{Co} = 0.53$ Å at CN=6), Fe^{3+} ($r_{Fe} = 0.55$ Å at CN=6 and low spin), Ni^{3+} ($r_{Ni} = 0.56$ Å at CN=6 and low spin), Mn^{3+} ($r_{Mn} = 0.58$ Å at CN=6 and low spin) and Cr^{3+} ($r_{Cr} = 0.56$ Å at CN=6). As can be seen from Table 1, lanthanum-cobalt-based oxides have the highest ionic conductivity among the disordered perovskites. However, cobalt-containing cathodes encounter some problems such as high thermal expansion coefficients (TECs) and poor stability as well as the high cost of cobalt. Partial substations of cobalt by other elements in cobalt-containing cathodes are considered a possible means to compensate for its disadvantages [87].

Fast diffusion of oxygen ions in ordered perovskites was first demonstrated by Taskin et al. [63, 66] on the samples of $GdBaMn_2O_{5+\delta}$ and $GdBaCo_2O_{5+\delta}$. In these materials the A cation lattice can be ordered and disordered depending upon the preparation conditions. It was shown that the oxygen diffusion coefficient is significantly enhanced when A-site cation order is achieved. This is explained by the crystallographic layers arising at transformation of simple cubic perovskite diminish the oxygen bonding strength and created disorder-free channels for ion motion [63]. At the same time, oxygen diffusion in layered perovskites is anisotropic. The oxygen transport takes place within the AO_δ planes and oxygen diffusion through the CoO_2 plane or in a direction perpendicular to the AO_δ plane is insignificant [88]. This fact was experimentally confirmed by investigation of epitaxial film of $GdBaCo_2O_{5\pm\delta}$ [89] and the ceramic sample of $PrBaCo_2O_{5\pm\delta}$ [90].

The main involved driving force for the layered structure formation is the ionic radii of the elements that constitute the compound. It is fundamental that the difference between the ionic radii of the elements occupying A- and A'-site is significant, otherwise the two cations will randomly distribute in a disordered $AA'BO_3$ lattice [36]. In a typical double perovskite a rare earth elements usually occupy the A site. In A'-site an element with appropriate dimension is required, and big ions such as barium or strontium were proposed. In this case, the use of a large ion of La as the A-site cation results in the formation of a disordered structure [54], therefore lanthanum-based perovskites are most often considered as simple perovskite with the general formula $A_{0.5}A'_{0.5}BO_3$. In ordered perovskites the most used elements as B-site cations are cobalt, manganese, iron and copper. Comparing the data of Tables 1 and 2, it can be seen that the ordered perovskites possess higher values of the diffusion coefficients than the disordered ones.

Theoretical studies [91] provided evidence that brownmillerite-type materials with ordered anion vacancies might present an enhanced ionic conductivity due

to energetically favored oxygen diffusion paths in particular crystallographic directions. However, high values of the ionic conductivity in these structures have not been obtained experimentally (see Table 2 [67, 68]). The migration energy in tetrahedral layers of the brownmillerite structure is substantially higher than in octahedral [92] and consequently the oxygen transport along the octahedral layers is most probable (Figure 4). Therefore, in [68], it was suggested that this insignificant ionic conductivity due to the low concentration of oxygen vacancies in the octahedral layers. Thus, the ionic conductivity of brownmillerite-type materials can be improved by suitable doping.

Most common representative of the simplest member of RP series is Ln_2NiO_4 (Ln=lanthanide). These oxides possess intrinsic oxygen ionic conductivity without the necessity of forming oxygen hypostoichiometry through ionic doping [93, 94]. The special transportation mechanism of oxygen ions in A_2BO_4 structure has been thoroughly investigated and a brief review this topic has been presented in [57]. It was predicted the oxygen diffusion in a lattice of the A_2BO_4 materials is anisotropic character: migration of the oxygen ions along plane (*a, b*) (rock-salt layer) is more preferable than along the axis *c* [95-98]. The data of works [69, 74, 99-102] confirmed the diffusion anisotropy. In particular for $La_2NiO_{4+\delta}$ single crystal it was be found the oxygen diffusion coefficient (D^*) along the (*a, b*) plane being about one to two orders of magnitude higher in compared to that along the perpendicular direction [99]. Moreover, the values of transport parameters determined on polycrystalline samples are close to the (*a, b*) plane, suggesting that the oxygen transport processes dominate in this plane for ceramic materials.

In [69] was shown that the diffusion coefficients (D^*) of the A_2BO_4 materials depends quite weakly on the change in the stoichiometry of oxygen. Since non-stoichiometry is mainly determined by the material composition it has been suggested that the partial substitutions of A and B-site cations has little effect on oxygen transport. In addition the results of simulation [103] indicate that nature of the B-site cation might not be expected to have a significant effect on oxygen diffusion due to its motion along A_2O_2 planes. As can be seen from Table 3, these assumptions are basically true (within the scatter of literature data).

The relationship between the diffusivity and the nature of the A cation has not been fully explored but it might be expected that the larger A cations result in a more open rock-salt layer [57]. If comparison of data for Ln_2NiO_4 (Ln = La, Pr, Nd) [70] (Table 3) it's clear that the diffusion coefficient decreases in the sequence Pr-Nd-La at its ionic radii of 1.17 Å (CN=9), 1.27 Å (CN=12) and 1.36 Å (CN=12), respectively. The same result was obtained in work [69].

High-order Ruddlesden-Popper phases of $A_3B_2O_7$ (n=2) and $A_4B_3O_{10}$ (n=3) began to studied relatively recently as potential oxygen reduction electrodes for SOFCs. Unfortunately, there is little research on this subject yet. It has been detail investigated only few compositions in the main on the basis of lanthanum-nickel and strontium-iron systems [75-78, 104-109]. As can be seen from Table 3, the ionic conductivity of $Sr_3Fe_2O_7$ is comparable with the best one for materials with a disordered perovskite structure. Partial substitution of Sr and Fe by La and Sc respectively results in a decrease of the ionic conductivity [76, 78], whereas the substitution of B-site cation by Co increases the ionic conductivity [76]. A

similar dependence was observed for the compositions of $LaSr_3Fe_{3-x}Co_xO_{10}$ ($0 \le x \le 1.5$) being n = 3 member of the RP series.

Thermal expansion

For cathode materials that are used in SOFC the thermal expansion becomes an important physical property, as mismatch of the thermal expansion of the cell components will cause early cell failure. The thermal expansion coefficient (TEC) of most common electrolytes of YSZ, GDC and LSGM are 10.0×10^{-6} K^{-1}, 12.5×10^{-6} K^{-1} and 10.4×10^{-6} K^{-1} respectively [110].

The thermal expansion coefficient of a solid is related to the asymmetries of the interatomic potential [19]. The magnitude of the thermal expansion of a lot of perovskites is determined by the thermal behavior of BO_6 octahedrons and associated with octahedral tilt, distortion, and bonding between the B-cation and the surrounding anions [30]. In addition, TEC depends on the magnetic and electronic transitions, and can also modification at a chemical composition change of the compound occurring with increasing temperature. Thus, at temperature growth the concentration of oxygen vacancies in oxides of transition metals is able to increase, which resilts in a decrease of the transition metal cation oxidation state and consequently in the elongation of the metal-oxygen bond. For example, TEC of $Sc_{0.75}Y_{0.25}Fe_{0.75}Co_{0.25}O_{3-\delta}$ increases from 14.6×10^{-6} K^{-1} to 22.1×10^{-6} K^{-1} at heating above 400 °C [111].

It was shown that there is the linear relation between $log\sigma_i$ (where σ_i is ionic conductivity) and TEC for perovskites of $A_{1-x}Sr_xBO_3$ (A=La, Pr, Ce; B=Mn, Fe, Co, Ni, Ga, Mg) [46]. Although other literary data do not always exactly correspond to the obtained dependence, the general trend persists. The highest values for both ionic conductivity and TEC are observed for strontium cobaltites and the lowest values for lanthanum manganites. The ordered perovskites show same dependence: Co-containing compositions have a high TEC. This is due to the presence of spin transitions between the low- (LS, $t_{2g}^6e_g^0$) and high-spin (HS, $t_{2g}^4e_g^2$) states of the Co^{3+} cation [112].The transition from LS to HS state is accompanied by a significant increase in the average Co-O bond length and the TEC value.

The ground state of Co^{3+} cation has to be HS in order to Co-containing complex oxide has a low TEC value. The Co spin state depends on the coordination environment. In the structure of $LaCoO_3$ disordered perovskite the $Co^{3+}+$ is exclusively in the LS state [113]. In $LaSrCoO_4$ material with the RP structure it is in a mixed (LS + HS) state [114]. Both in the $GdBaCo_2O_{5.5}$ layered perovskite [115] and in the $Sr_2Co_{2-x}GaO_5$ brownmillerite [116], the HS state stabilizes. Therefore, the TEC of these compounds has a low value. For example the TEC of $Sr_2Co_2O_5$ is 11.7×10^{-6} K^{-1} at 25-400°C [117]. Thus, ordered perovskites and RP phases generally possess a smaller TEC as compared to disordered perovskites (see Tables 1-3).

Another way to tailoring of TEC is changing the composition of the material via A-, B- site substitution. In this case, the common dependence is observed for

all structures under consideration: the substitution of Co by Mn, Fe reduces TEC value. However, the substitution also results in a decrease in both the electron and ionic conductivity. Therefore, at development of SOFC cathode material, it is necessary to find a compromise between high electrical and suitable thermal properties.

Conclusion

At present time perovskites and perovskite-related materials is considerable interest as the promising cathode materials for SOFC. The brief review carried out in this paper showed that materials with the structure of the disordered cubic perovskite possess the highest electronic conductivity. On the other hand the layered perovskites and materials with the Ruddlesden-Popper structure have high values of ionic conductivity because the ion transport is facilitated due to the features of the crystal structure. TEC of these materials is generally closer to TEC of the electrolytes in comparison with the disordered perovskite one.

Unfortunately, it is now impossible to point out any composition or structure as an ideal candidate for the cathode material. The flexibility of perovskite structures with respect to doping implies the existence of a huge number of unstudied compounds. We hope that the general structure-properties patterns covered in this paper will help in finding the desired cathode material.

Acknowledgments

References

[1] J.T.S. Irvine and P. Connor, Solid Oxide Fuels Cells: Facts and Figures (Springer-Verlag, London, 2013) 230 p.
[2] S.C. Singhal and K. Kendall, High Temperature Solid Oxide Fuel Cells: Fundamentals, Design and Applications (Elsevier, Oxford, 2003) 405 p.
[3] M. Koyama et al., J. Electrochem. Soc. **147**(1) (2000) 87.
[4] M. Ni et al., Fuel Cells **7** (2007) 269.
[5] S.P. Jiang, J. Mater. Sci. **43** (2008) 6799.
[6] N.Q. Minh, Journal of the American Ceramic Society **76**(3) (1993) 563.
[7] S.P. Jiang, Solid State Ionics **146**(1) (2002) 1.
[8] I. Yasuda, K. Ogasawara et al., Solid State Ionics **86**(2) (1996) 1197.
[9] K. Sasaki, J.P. Wurth et al., Electrochem. Soc. **143**(2) (1996) 530.
[10] S.B. Adler, Chem. Rev. **104**(10) (2004) 4791.
[11] T.Z. Sholklapper, H. Kurokawa et al., Nano Letters **7**(7) (2007) 2136.

[12] Y. Takeda et al., Electrochem. Soc. **134** (1987) 2656.

[13] C. Sun et al., Journal of Solid State Electrochemistry **14**(7) (2010) 1125.

[14] N. Mahato, A. Banerjee et al., Progress in Mater. Sci. **72** (2015) 141.

[15] M. Yuste et al., Dalton Trans. **40** (2011) 7908.

[16] B.C.H. Steele, Solid State Ionics **86** (1996) 1223.

[17] S.B.Adler et al., J. Electrochem. Soc. **143** (1996) 3554.

[18] B.C.H.Steele, Solid State Ionics **134**(1-2) (2000) 3.

[19] S.Ya. Istomin et al, Russ. Chem. Rev. **82** (2013) 686.

[20] A.S. Bhalla et al., Mat. Res. Innovat. **4** (2000) 3.

[21] G. King, P.M. Woodward, Mater. Chem. **20**(28) (2010) 5785.

[22] S. Vasala, M. Karppinen, Progress in Solid State Chemistry **43**(1) (2015) 1.

[23] B.V. Beznosikov, K.S. Aleksandrov, Crystallography Reports **45**(5) (2000) 792.

[24] A.M. Abakumov, M.G. Rozova et al., Russ. Chem. Rev. **73**(9) (2004) 847.

[25] J. Young, J.M. Rondinelli, Physical Review B **92**(17) (2015) 174111.

[26] V.M. Goldschmidt, Naturwissenschaften **14**(21) (1926) 477.

[27] A.M. Glazer, Acta Crystallogr. Sect. B **28** (1972) 3384.

[28] P.M. Woodward, Acta Crystallogr. Sect. B **53** (1997) 32.

[29] C.J. Howard, H.T.Stokes, Acta Crystallogr. Sect. B **54** (1998) 782.

[30] R.J.D. Tilley, Perovskites. Structure-Property Relationships (John Wiley & Sons Ltd., UK, 2016) 315 p.

[31] S.N. Ruddlesden, P. Popper, Acta Cryst. **11** (1958) 54.

[32] S. Yoo, S. Choi et al., RSC Adv. **2** (2012) 4648.

[33] J. Richter, P. Holtappels et al. Monatsh. Chem. **140**(9) (2009) 985.

[34] J. Sunarso, S.S. Hashim et al., Prog. Energy Combust Sci. **61** (2017) 57.

[35] H. Kozuka, K. Ohbayashi et al., Sci. Technol. Adv. Mater. **16** (2015) 026001.

[36] R. Pelosato, G. Cordaro et al., J. Power Sources **298** (2015) 46.

[37] D.Z. de Florio, F.C. Fonseca et al., Ceramica **50**(316) (2004) 275.

[38] A.V. Berenov et al., Solid State Ionics **122**(1) (1999) 41.

[39] T. Ishigaki, S. Yamauchi et al. Solid State Chem **55**(1) (1984) 50-53.

[40] W.Z. Zhu, S.C. Deevi, Mater. Sci. and Engineering A **328** (1) (2003) 227.

[41] T. Ishigaki, S. Yamauchi et al. Solid State Chem. **54**(1) (1984) 100.

[42] V. Oygarden, T. Grande, Dalton Trans. **42**(8) (2013) 2704.

[43] Y. Teraoka, H.M. Zhang et al., Mat. Res. Bull. **23**(1) (1988) 51.

[44] L.-W. Tai, M.M. Nasrallah et al., Solid State Ionics **76**(3) (1995) 259.

[45] A. Petric, P. Huang, F. Tietz, Solid State Ionics **135**(4) (2000) 719.

[46] H. Ullmann, N. Trofimenko et al., Solid State Ionics **138**(1) (2000) 79.

[47] F. Tietz, I. A. Raj et al. Prog Solid State Chem. **35** (2007) 539.

[48] F. Tietz, I. A. Raj et al. Solid Sate Ionics **177** (2006) 1753.

[49] S.I. Benson, R.J. Chater et al., Ionic and mixed conducting ceramic III, in Electrochemical Society Proceedings (1998) 596.

[50] Ch. Ftikos, S. Carter et al., J. Eur. Ceram. Soc. **12**(1) (1993) 79.

[51] A. Mahata, P. Datta, R.N. Basu, Ceram Int. **43**(1) (2017) 433.

[52] V.V. Kharton, A,A. Yaremchenko et al., Solid State Electrochem. **3** (1999) 303.

[53] J. M. Serra, V.B. Vert et al., J. Electrochem. Soc. **155**(2) (2008) B207.

[54] J.H. Kim, A. Manthiram, Electrochem. Soc. **155**(4) (2008) B385.

[55] Q. Zhou, W.C.J. Wei et al., Electrochem. Commun. **19** (2012) 36.

[56] L. Jiang, F. Li et al., Electrochim. Acta **133** (2014) 364.
[57] A. Tarancon, M. Burriel et al., J. Mater. Chem. **20**(19) (2010) 3799.
[58] G. Kim, S. Wang et al, J. of Materials Chemistry **17** (2007) 2500.
[59] H.T. Lozano, J. Druce et al., Sci. Technol. Adv. Mater. **18**(1) (2017) 977.
[60] F. Jin, H. Xu et al., J. Power Sources **243** (2013) 10.
[61] L. Zhao, J. Shen et al., Int. J. Hydrogen Energy **36**(5) (2011) 3658.
[62] Y. Wang, X. Zhao et al., Ceram. Int. **40**(7) (2014) 11343.
[63] A.A. Taskin, A. N. Lavrov, Y. Ando, App. Physics Letters **86** (2005) 091910 .
[64] A. Tarancon, S. J. Skinner et al., J. of Materials Chemistry **17**(2007) 3175.
[65] J. Fleig, J. Power Sources **105**(2) (2002) 228.
[66] A.A. Taskin et al., Progress in Solid State Chemistry **35** (2007) 481.
[67] K.R. Kendall, C. Navas et al., Solid State Ionics **82**(3) (1995) 215.
[68] A.L. Shaula, Y.V. Pivak et al., Soli State Ionics **177**(33-34) (2006) 2923.
[69] E. Boehm, J.-M. Bassat et al., Solid State Ionics **176**(37) (2005) 2717.
[70] H. Zhao, Q. Li et al. Sci. China Chem. **54** (2011) 898.
[71] E.V. Tsipis, V.V. Kharton, J. Solid State Electrochem. **15**(5) (2011) 1007.
[72] S.J. Skinner, J.A. Kilner, Solid State Ionics **135**(4) (2000) 709.
[73] M.Al Daroukh, V.V. Vashook et al., Solid State Ionics **158**(1) (2003) 141.
[74] C.N. Munnings, S.J. Skinner, et al. Solid State Ionics **176**(23) (2005) 1895.
[75] G. Amow, S. J. Skinner, J. Solid State Electrochem. **10**(8) (2006) 538.
[76] F. Prado, T. Armstrong et al., J. Electrochem. Soc. **148**(4) (2001) J7.
[77] M.V. Patrakeev, I.A. Leonidov et al., Solid State Sci. **6**(9) (2004) 907.
[78] A.A. Markov, M.V. Patrakeev et al., Chem.Mater. **19**(16) (2007) 3980.
[79] J. Mizusaki, I. Yasuda et al., J. Electrochem. Soc. **140**(2) (1993) 467.
[80] J. Mizusaki, N. Mori et al., Solid State Ionics **129**(1-4) (2000) 163.
[81] A.N. Petrov, O.F. Kononchuk et al., Solid State Ionics **80**(3-4) (1995) 189.
[82] H. Hayashi, H. Inaba, et al., Solid State Ionics **122**(1-4) (1999) 1.
[83] M. Mogensen, D. Lybye et al., Solid State Ionics **174**(1-4) (2004) 279.
[84] J. C. Boivin, G. Mairesse, Chem. Mater. **10**(10) (1998) 2870.
[85] H. Iwahara, T. Esaka et al., Solid State Ionics **3/4** (1981) 359.
[86] H. Iwahara, H. Uchida et al., J. Electrochem. Soc. **135**(2) (1988) 529.
[87] H. Ding, X. Xue, Electrochim. Acta. **55**(11) (2010) 3812.
[88] K. Zhang, L. Ge, et al., Acta Mater. **56**(17) (2008) 4876.
[89] Zapata, J., Burriel, M. et al. Mater. Chem. A. **1**(25) (2013) 7408.
[90] M. Burriel, J. Pe?a-Mart?nez et al. Chem. Mater. **24**(3) (2012) 613.
[91] C.A.J. Fisher, M. S. Islam, Solid State Ionics **118**(3-4) (1999) 355.
[92] C.A.J. Fisher, M.S. Islam, J. Mater. Chem. **15** (2005) 3200.
[93] D. Parfitt, A. Chroneos et al., Phys. Chem. Chem. Phys. **12**(25) (2010) 6834.
[94] H. S.Kim, H.I. Yoo, Phys. Chem. Chem. Phys. **13**(10) (2011) 4651.
[95] N.L. Allan, W.C. Mackrodt, Philos. Mag. A **64**(5) (1991) 1129.
[96] M.S.D. Read, M.S. Islam et al., J. Phys. Chem. B **103** (9) (1999) 1558.
[97] L. Minervini, R. W. Grimes et al., J. Mater. Chem. **10** (2000) 2349.
[98] A.R. Cleave, J.A. Kilner et al., Solid State Ionics **179**(21-26) (2008) 823.
[99] J.M. Bassat, P. Odier et al., Solid State Ionics **167**(3-4) (2004) 341.
[100] M. Yashima, M. Enoki, et al., J. Am. Chem. Soc. **130**(9) (2008) 2762.
[101] J.M. Bassat, M. Burriel et al., J. Phys. Chem. C **117**(50) (2013) 26466.

[102] M. Burriel, G. Garcia et al., J. Mater. Chem. **18** (2008) 416.

[103] A. Chroneos, D. Parfitt et al., J. Mater. Chem. **20** (2010) 266.

[104] R.J. Woolley, M.P. Ryan et al. Fuel Cells **13**(6) (2013) 1080.

[105] G. Amow, I. Davidson et al., Solid State Ionics **177**(13-14) (2006) 1205.

[106] M. Burriel, G. Garcia et al., J. Santiso , Chem. Mater. **19**(16) (2007) 4056.

[107] S. Takahashi, S. Nishimoto et al. J. Am. Ceram. Soc. **93**(8) (2010) 2329.

[108] Z. Lou, J. Peng et al. Electrochem. Commun. **22** (2012) 97.

[109] G. Amow, J. Au et al. Solid State Ionic **177**(19-25) (2006) 1837.

[110] E.V. Tsipis, V.V. Kharton, J. Solid State Electrochem. **12**(9) (2008) 1039.

[111] S.Ya. Istomin, et al., Solid State Ionics **179**(21-26) (2008) 1054.

[112] S. Park, S. Choi et al., Electrochim. Acta **125** (2014) 683.

[113] Z. Hu, H. Wu et al., Phys. Rev. Lett. **92**(20) (2004) 207402.

[114] J. Wang, W. Zhanget al., Phys. Rev. B: Condens. Matter **62** (2000) 14140.

[115] M.Garcia-Fernandez et al., Phys. Rev. B: Condens. Matter **78** (2008) 054424.

[116] P.G.Radaelli and S.-W.Cheong, Phys. Rev. B: Condens. Matter **66** (2002) 094408.

[117] C.de la Calle, A.Aguadero et al., Solid State Sci. **10**(12) (2008) 1924.